Bond failure of a SiC/SiC brazed assembly

Leminh Nguyen, Dominique Leguillon, Olivier Gillia, Emmanuelle Rivière

Bond failure of a SiC/SiC brazed assembly

L.M. Nguyen [a,1], D. Leguillon [b,*], O. Gillia [a,2], E. Riviere [c,3]

[a] CEA/LITEN/DTBH/LTH, 17 rue des Martyrs, 38054 GRENOBLE CEDEX 09, France
[b] Institut JLRA – CNRS UMR 7190, Université Pierre & Marie Curie (Paris 6), 4 place Jussieu, 75252 PARIS CEDEX 05, France [c] CNES/DCT/TV/MT, 18 avenue Edouard Belin, 31401 TOULOUSE CEDEX 09, France

The failure initiation of a brazed structure made of Silicon Carbide components is analysed by means of a two-scale analysis and a twofold failure criterion using both a maximum released energy and a maximum tensile stress conditions. In a first step, two asymptotic expansions are settled to describe the perturbation caused by the emergence of the thin solder layer on the free edge surface of the structure, at the macro and micro levels. The resulting far field evidences a logarithmic term. This is mainly due to different elastic properties of the two materials leading to a conflicting necking effect. In a second step, the fail-ure criterion is established; the two conditions lead to two branches depending on the thickness of the solder layer, one is governed by the energy condition and the other by the stress condition. Predictions agree almost well with experiments carried out at room temperature on brazed specimens of SiC with different Silicon based solders.

1. Introduction

Silicon Carbide (SiC) based structures are widely used in the space industry (Bath et al., 2005) thanks to the mechanical and thermal properties of this material and its chemical stability. They are now used in high temperature heat exchangers for energy conversion or in chemical reactors (Lewinsohn et al., 2000; Rodriguez et al., 2007). However, the manufacturing process (sintering) does not allow the production of very large elements such as mirrors for satellite (Herschel mirror for instance) or very complex geometries. Therefore it is necessary to build piece by piece and to use an assembly method. Brazing currently seems the most appropriate, using a filler material with properties as close as possible to the substrates to avoid incompatibility problems (Katoh et al., 2000; Riccardi et al., 2002a). The process called BraSiC® uses Silicon combined with a metal component as filler, the bonding is made at high temperature (≈1400 °C) and impregnation is achieved by gravity/capillarity (Gasse, 2003; Gasse et al., 2003).

For the safety of these facilities, the most important question that arises is the mechanical resistance of the assembly. To this aim, a 4-point bending test campaign on bars assembled end-to-end was conducted at room temperature. It led to analyze the role of a key parameter: the thickness of the butt joint which was varied from 3 to 200 μm.

This experimental work was accompanied by a theoretical model based on the use of a failure coupled criterion (Leguillon, 2002) (i.e. using both energy and stress conditions). It was exploited to highlight the role of the thickness of the solder joint in tests on brazed bars, resulting in a very simple formula in perfect agreement with the experimental results: strength is proportional to the inverse of the square root of the solder joint thickness.

The present paper is devoted to a brief description of the experiments and to a theoretical model of fracture. This model relies on an asymptotic approach which allows getting rid of time consuming finite element computations car-

* Corresponding author. Tel.: +33 1 44 27 53 22.

E-mail addresses: nguyenleminhbk@gmail.com (L.M. Nguyen), dominique.leguillon@upmc.fr (D. Leguillon), olivier.gillia@cea.fr (O. Gillia), emmanuelle.riviere@cnes.fr (E. Riviere).

[1] Tel.: +33 4 38 78 03 83.
[2] Tel.: +33 4 38 78 62 07.
[3] Tel.: +33 5 61 28 30 88.

ried out on strongly refined meshes within and around the joint (Nguetseng and Sanchez-Palencia, 1985; Leguillon, 1995; Leguillon and Abdelmoula, 2000; Haboussi et al., 2001). The fracture criterion is based on a twofold condition in energy and stress (Leguillon, 2002). It splits into two branches, one is governed by the energy condition, it is associated with the thinner solder layers. The other one, governed by the stress condition, corresponds to thicker layers. The predictions agree almost well with the experimental measures derived from the experiments carried out on various grades of brazing material.

A point is not studied here, taking into account the thermal residual stresses due to the process used for making the joint. Tests conducted at high and low temperatures failed to clearly demonstrate their role as several authors have found (Singh, 1997; Riccardi et al., 2002b; Cockeram, 2005; Nguyen, 2011) even if thermal expansion coefficients are significantly different. Anyway, these thermal stresses remain transparent to the identification procedure necessary to the failure prediction we use.

2. The experiments – 4-point bending tests

According to the standards NF EN 843-1 (2007) and ASTM C1211-02 (2008) for flexural monolithic ceramics, we used a specially designed fixture to avoid friction and alignment problems (Fig. 1). The load rate was set to 0.5 mm/min and data collection was performed using Testworks software. The peak load reported by the software was used to calculate the flexural strength. The outer and the inner span lengths were 40 mm and 20 mm, respectively.

The test specimens were made of two bars of SiC joined together by using 2 different grades of brazing material BraSiC® baptized CEA1 and CEA2. The Young modulus of SiC was taken from the literature $E = 416$ GPa and that of the brazing material was determined by nano-indentation $E = 154 \pm 8$ GPa for CEA1 and $E = 171 \pm 23$ GPa for CEA2. An average value $E = 160$ GPa was selected for the numerical simulations.

Specimens for bending tests were machined from butt joined plates. The joint was located in the middle of the flexure bars. Dimensions of specimens were respectively $4 \times 3 \times 46$ mm^3. The thickness of the joint was varied from 3 ± 1 μm to 200 ± 10 μm. Then, all surfaces were grinded
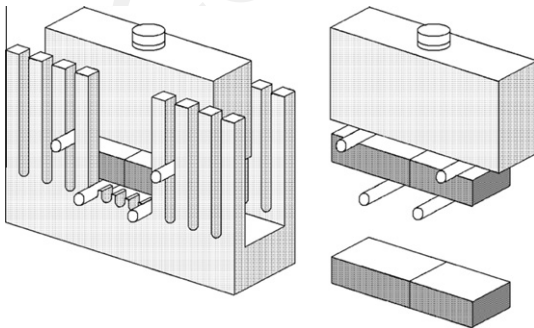
Fig. 1. The 4-point bending device according to standards NF EN 843-1 and ASTM C1211-02 and the butt jointed SiC sample (the scale is not fully respected).

and small chamfers were made on the edges of the tensile surface of the specimen. However, specimens without chamfer were also used and it was verified that this had no influence on the fracture results. The stress T acting along the tensile surface was calculated from the classical (1) corresponding to the bending of a beam submitted to a homogenous 4-point bending remote load

$$T = \frac{3F(L - l)}{2bh^2} \tag{1}$$

where F is the maximum load (N), L the outer span distance (mm), l the inner span distance (mm), b the beam width (mm) and h the beam thickness (mm) (Fig. 2(a)). A minimum of 7 specimens were tested for each bond thickness at room temperature in air. After testing, fracture surfaces were examined by optical and scanning electron microscopy to identify the failure origin.

The room-temperature flexural strengths of brazed SiC specimens are shown in Section 8, Figs. 9 and 10. They exhibit a flexural strength close to the bulk tensile strength of SiC (around 496 ± 91 MPa) for very thin joints and a big significant change as a function of the joint thickness e.

For CEA1, a rapid decrease of the bending strength to 194 ± 42 MPa was recorded when thickness varies from 3μ to 19μ. For a joint thickness around 93 μm, flexural strength decreases to 115 ± 42 MPa with a smaller slope.

Under similar test conditions, the joined CEA2 specimens with different thickness of joint of 3 μm, 18.6μ, 91 μm had bending strengths of 368 ± 72 MPa, 148 ± 23 MPa and 123 ± 24 MPa, respectively. The CEA1 joint shows a better strength than CEA2, especially for small thicknesses.

For very thin joints (3 ± 1 μm), there are 5 and 11 out of 14 tested specimens (respectively for CEA1 and CEA2 solders) for which failure occurs in the brazing joint (we called failure in the brazing joint when failure occurs within the joint or along its interfaces with the SiC substrate). The other failures occur at the loading rollers or close to them. Obviously, resistance of thin joints is almost as strong as SiC and the standard deviations overlap, thus possibility of failure either in the joint or in the SiC substrate likely depends where the most critical defect is.

3. The theoretical model and a first step in the matched asymptotic procedure

As is desired in industrial processes, the joint thickness e must be small compared to the overall dimensions of the samples ($e \ll h$ beam thickness, $e \ll L$ beam length, Fig. 2). Considering these joints in a finite elements analysis (FEA) implies the use of strongly refined meshes inside and in their vicinity. This section and the next two are devoted to the description of a matched asymptotic procedure with respect to e which allows getting rid of this drawback. It is based on a two-scale approach. In the so-called outer or macro one the joint thickness is neglected, as it is tempting to do because of it smallness, whereas in the inner or micro approach the joint has a finite thickness but the exact geometry of the samples is neglected. Moreover the latter problem can be solved once and for all, whatever the global geometry of the specimen and whatever the mode of
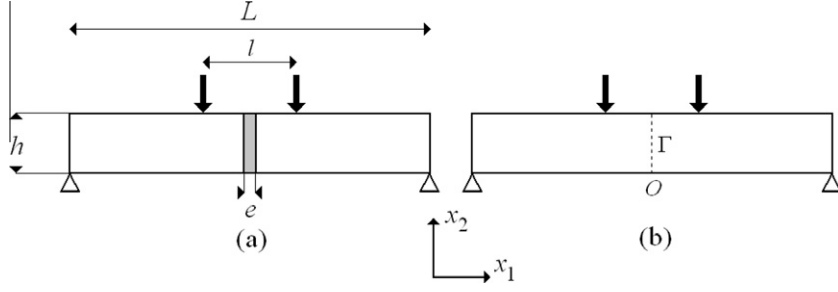
Fig. 2. Schematic view of the butt joined specimen under a 4-point bending load (a) and the simplified problem neglecting the joint thickness (b). The virtual interface Γ ($x_1 = 0$) between the left and right parts of the specimen is highlighted.

loading and its intensity. In addition, this two-scale approach allows evidencing some significant parameters which intervene in the fracture process.

We consider specimens made of two parts of a stiff elastic material with Lamé's coefficient $\lambda^S = 84.4$ GPa and $\mu^S = 179.3$ GPa (the index S denotes the two SiC bars with $E = 416$ GPa, $\nu = 0.16$). They are bonded together by a thin solder layer with thickness e (assumed to be far smaller than the specimen size $e \ll L$ and $e \ll h$) and Lamé's coefficient $\lambda^L = 228.6$ GPa and $\mu^L = 57.2$ GPa (the index L corresponds to the BraSiC® layer with $E = 160$ GPa, $\nu = 0.4$). They form the domain Ω^e (Fig. 2a). In the experiments, they are submitted to a 4-point bending loading (Fig. 2) but it is clear that the same reasoning works for any other problem, a tensile loading for instance.

Under plane strain assumption, the solution to the elastic problem in Ω^e is searched in the form of a so-called outer expansion (Nguetseng and Sanchez-Palencia, 1985)

$$\underline{U}^e(x_1, x_2) = \underline{U}^0(x_1, x_2) + e\underline{U}^1(x_1, x_2) + e^2\underline{U}^2(x_1, x_2) + \cdots \quad (2)$$

where the dots $\cdots$ hold for terms smaller than e^2. The successive terms are solution to problems settled on the simplified domain $\Omega^0 = \lim_{e \to 0} \Omega^e$ where the bonding layer is not visible (Fig. 2b). Obviously, such an approximation is valid only out of a vicinity of the virtual interface Γ, which explains the name "outer".

The first term $\underline{U}^0(x_1, x_2)$ is continuous through the line Γ and fulfils the classical set of equations of a 4-point bending test on a homogeneous isotropic sample (Fig. 2(b)). The solution can be either approximated analytically (Eq. (1)) or easily solved by a FEA without special requirements on the mesh.

In the vicinity of the origin O this leading term can be expanded using the uniform tension in direction x_1 expressed below in polar variables (throughout this paper Cartesian coordinates (x_1, x_2) and polar ones (r, θ) both with origin at O are unambiguously mixed)

$$\underline{U}^0(x_1, x_2) = \underline{U}^0(O) + Tr\underline{t}^1(\theta) + \cdots \quad (3)$$

with

$$\begin{cases} rt_1^1(\theta) = r\frac{\lambda^S + 2\mu^S}{4\mu^S(\lambda^S + \mu^S)}\cos\theta = \frac{\lambda^S + 2\mu^S}{4\mu^S(\lambda^S + \mu^S)}x_1 \\ rt_2^1(\theta) = -r\frac{\lambda^S}{4\mu^S(\lambda^S + \mu^S)}\sin\theta = -\frac{\lambda^S}{4\mu^S(\lambda^S + \mu^S)}x_2 \end{cases} \quad (4)$$

The coefficient T is the tension on the lower face of Ω^0 as estimated in the experiments (Eq. (1) for instance). The associated stress field fulfils

$$\sigma_{11}^1(r, \theta) = T; \quad \sigma_{12}^1(r, \theta) = \sigma_{22}^1(r, \theta) = 0 \quad (5)$$

The first term of (3) is an irrelevant constant corresponding to the vertical deflection of point O. According to the singularity theory (Leguillon and Sanchez-Palencia, 1987), the remaining terms in (3) involve higher integer powers of the space variable r.

The next terms of expansion (2) result more precisely of a matched asymptotic procedure as presented in Sections 4 and 5.

4. The inner expansion

To have more details on the region surrounding the origin O where a crack is expected to appear, a zoom in is carried out. But contrarily to the usual procedure (Haboussi et al., 2001) in such situation which consists in stretching the initial domain in the single direction x_1, we consider a dilatation in all directions around the origin O: $x_i \to y_i = x_i/e$ ($i = 1, 2$) (in polar coordinates $r \to \rho = r/e$). In this domain an inner expansion (as opposed to the previous outer one) is assumed in the following form

$$\underline{U}^e(x_1, x_2) = \underline{U}^e(ey_1, ey_2)$$
$$= \underline{W}^0(y_1, y_2) + e\,\underline{W}^1(y_1, y_2) + \cdots \quad (6)$$

The successive terms in (6) are solutions to problems settled in the unbounded (as $e \to 0$) domain Ω^{in} spanned by the pair y_1 and $y_2 \geqslant 0$. Clearly, finite values of y_1 and y_2 correspond to small values of x_1 and x_2. Thus the expansion (6) is valid in a vicinity of the solder layer, i.e. within a vertical band containing the solder joint (Fig. 3).

The two expansions Eqs. (2) and (6) are complementary, the matching conditions in between state that the solution in the inner domain Ω^{in} as one moves far from the origin (i.e. as $\rho \to \infty$) must match with the solution in the outer domain when approaching the origin O and the solder layer figured by the virtual line Γ (i.e. as $r \to 0$). In other words there is an intermediate region where the two expansions coincide. Thus, it can be easily derived that $\underline{W}^0(y_1, y_2)$ must behave like $\underline{U}^0(O)$ and $\underline{W}^1(y_1, y_2)$ like $r\underline{t}^1(\theta)$ at infinity. Using the derivation rule $\partial * / \partial x_i = 1/e\ \partial * / \partial y_i$ for $i = 1, 2$, there is a trivial solution to the first condition

3
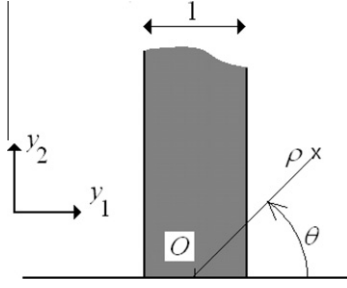
Fig. 3. The unbounded half space Ω^{in} spanned by y_1 and $y_2 \geqslant 0$, so-called inner domain.

$$\underline{W}^0(y_1, y_2) = \underline{U}^0(O) \tag{7}$$

And the second one can be ensured by superposition

$$\underline{W}^1(y_1, y_2) = T\rho \, \underline{t}^1(\theta) + \underline{\widehat{W}}^1(y_1, y_2) \tag{8}$$

The complementary term $\underline{\widehat{W}}^1(y_1, y_2)$ is decreasing to 0 at infinity.

For simplicity, in a first step, the stress free boundary conditions along the bottom face of the specimen are omitted, only interior points $y_2 > 0$ are considered. Then, according to the elastic equations, $\underline{\widehat{W}}^1(y_1, y_2)$ must be constant in the right and left parts of the SiC substrate (i.e. $y_1 \geqslant 1/2$ and $y_1 \leqslant -1/2$). By continuity and for symmetry reasons it comes (see Fig. 4)

$$\begin{cases} W_2^1(y_1, y_2) = -T\frac{\lambda^S}{4\mu^S(\lambda^S + \mu^S)}y_2 & \text{for any } y_1 \\ W_1^{1\pm}(y_1, y_2) = T\left(\frac{\lambda^S + 2\mu^S}{4\mu^S(\lambda^S + \mu^S)}y_1 \pm \frac{A}{2}\right) & \text{respectively for } y_1 \geqslant 1/2 \text{ and } y_1 \leqslant -1/2 \\ W_1^1(y_1, y_2) = T\left(\frac{\lambda^S + 2\mu^S}{4\mu^S(\lambda^S + \mu^S)} + A\right)y_1 & \text{for } -1/2 \leqslant y_1 \leqslant 1/2 \end{cases} \tag{9}$$

Eq. (9)$_1$ holds in the whole domain (the SiC substrate and the solder layer), Eq. (9)$_2$ holds in the right (upper index +) and in the left (upper index −) parts of the SiC substrate and Eq. (9)$_3$ in the solder layer. The constant A must be adjusted to ensure the stress vector continuity through the interfaces layer/substrate located at $y_1 = \pm 1/2$
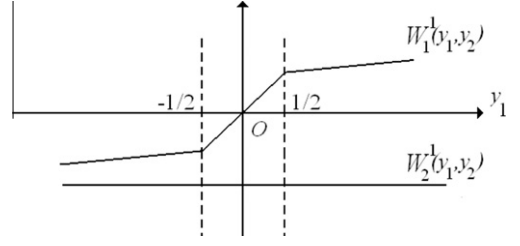
$$A = \frac{1}{\lambda^L + 2\mu^L} - \frac{1}{\lambda^S + 2\mu^S}$$
$$- \frac{\lambda^S}{4\mu^S(\lambda^S + \mu^S)}\left(\frac{\lambda^S}{\lambda^S + 2\mu^S} - \frac{\lambda^L}{\lambda^L + 2\mu^L}\right) \tag{10}$$

Then according to Eqs. (8) and (9)

$$\underline{\widehat{W}}^1(y_1, y_2) = T\underline{A}(y_1, y_2) \tag{11}$$

where the function $\underline{A}(y_1, y_2)$ is introduced allowing a more concise notation

$$\begin{cases} A_2(y_1, y_2) = 0 & \text{for any } y_1 \\ A_1(y_1, y_2) = \pm A/2 & \text{respectively for } y_1 \geqslant 1/2 \text{ and } y_1 \leqslant -1/2 \\ A_1(y_1, y_2) = Ay_2 & \text{for } -1/2 \leqslant y_1 \leqslant 1/2 \end{cases} \tag{12}$$

Fig. 4. The shape of the second term (9) of the inner expansion at an interior point, i.e. for a fixed value of $y_2 > 0$.

Now considering the boundary condition omitted in (9), it comes.

$$\begin{cases} \sigma_{12}(y_1, 0) = \mu^S\left(\frac{\partial W_1^1}{\partial y_2}(y_1, 0) + \frac{\partial W_2^1}{\partial y_1}(y_1, 0)\right) = 0 & \text{for } y_1 \leqslant -1/2 \text{ and } y_1 \geqslant 1/2 \\ \sigma_{22}(y_1, 0) = (\lambda^S + 2\mu^S)\frac{\partial W_2^1}{\partial y_2}(y_1, 0) + \lambda^S\frac{\partial W_1^1}{\partial y_1}(y_1, 0) = 0 & \text{for } y_1 \leqslant -1/2 \text{ and } y_1 \geqslant 1/2 \\ \sigma_{12}(y_1, 0) = \mu^L\left(\frac{\partial W_1^1}{\partial y_2}(y_1, 0) + \frac{\partial W_2^1}{\partial y_1}(y_1, 0)\right) = 0 & \text{for } -1/2 \leqslant y_1 \leqslant 1/2 \\ \sigma_{22}(y_1, 0) = (\lambda^L + 2\mu^L)\frac{\partial W_2^1}{\partial y_2}(y_1, 0) + \lambda^L\frac{\partial W_1^1}{\partial y_1}(y_1, 0) = TB & \text{for } -1/2 \leqslant y_1 \leqslant 1/2 \end{cases} \tag{13}$$

with

$$B = \frac{\lambda^L}{\lambda^L + 2\mu^L} - \frac{4\mu^L(\lambda^L + \mu^L)}{4\mu^S(\lambda^S + \mu^S)}\frac{\lambda^S}{\lambda^L + 2\mu^L} \tag{14}$$

This term vanishes only if

$$\frac{\lambda^S}{4\mu^S(\lambda^S + \mu^S)} = \frac{\lambda^L}{4\mu^L(\lambda^L + \mu^L)} \tag{15}$$

i.e. not surprisingly if the necking is the same in the substrate and in the layer. This is unlikely as soon as a significant contrast exists between the two materials. The inner solution (9) does not extend to the ends of the solder layer where it breaks the free surface.

Then an additional term $\underline{\widehat{\widehat{W}}}^1(y_1, y_2)$ must compensate the boundary condition imbalance (13)$_4$

$$\hat{\sigma}_{22}(y_1, 0) = (\lambda^L + 2\mu^L)\frac{\partial \widehat{W}_2^1}{\partial y_2}(y_1, 0) + \lambda^L\frac{\partial \widehat{W}_1^1}{\partial y_1}(y_1, 0)$$
$$= -TB \text{ for } -1/2 \leqslant y_1 \leqslant 1/2 \tag{16}$$

Such a problem is ill-posed. The resultant force $-TB \times 1$ (the stretched solder layer thickness is 1) extracted from (16) does not vanish and the solution cannot decrease to 0 at infinity as expected. It behaves like the point force solution $\underline{F}(y_1, y_2)$ involving a logarithmic term which can be written as (Timoshenko and Goodier, 1951)

$$\begin{cases} F_1(y_1, y_2) = -\frac{B}{\pi}\left(\frac{1}{2\mu^S}\sin\theta\cos\theta + \frac{1}{2(\lambda^S + \mu^S)}\theta - \frac{\pi}{4(\lambda^S + \mu^S)}\right) \\ F_2(y_1, y_2) = \frac{B}{\pi}\left(\frac{\lambda^S + 2\mu^S}{2\mu^S(\lambda^S + \mu^S)}\right)\ln\rho + \frac{B}{\pi}\left(\frac{\lambda^S}{2\mu^S(\lambda^S + \mu^S)}\cos^2\theta - \frac{1}{2(\lambda^S + \mu^S)}\sin^2\theta\right) \end{cases} \tag{17}$$

The corresponding resultant force vanishes in direction 1 and equals B in direction 2.

Since $\underline{F}(y_1, y_2)$ is singular both for $\rho \to 0$ and $\rho \to \infty$, the displacement field $\underline{\widehat{W}}^1(y_1, y_2)$ is rewritten by truncation and superposition

$$\underline{\widehat{W}}^1(y_1, y_2) = T\left(\underline{A}(y_1, y_2) + \varphi(\rho)\underline{F}(y_1, y_2) + \underline{\widehat{\widehat{W}}}^1(y_1, y_2)\right) \tag{18}$$

4

where $\varphi(\rho)$ is smooth enough and fulfils $\varphi(\rho) = 0$ if $\rho < \rho_1$ and $\varphi(\rho) = 1$ if $\rho > \rho_2$ (ρ_1 and ρ_2 are arbitrarily chosen so that $\rho_2 > \rho_1$). The function $\varphi(\rho)$ allows getting rid of the singular behaviour of $\ln\rho$ at the origin ad ensure the right behaviour at infinity. The function $\widehat{\widetilde{W}}^1(y_1, y_2)$ is solution to a well-posed problem with vanishing conditions at infinity. More precisely it behaves like $1/\rho$, the associated mode is a kind of pinching $1/\rho \underline{t}^{-1}(\theta)$ (Leguillon and Sanchez-Palencia, 1990). The notation $\underline{t}^{-1}(\theta)$ is used to recall that this mode is the so-called dual mode (Leguillon and Sanchez-Palencia, 1987) to $\underline{t}^1(\theta)$ defined in (4)

$$\begin{cases} t_\rho^{-1}(\theta) = \frac{\cos 2\theta}{\mu^S} \\ t_\theta^{-1}(\theta) = -\frac{\sin 2\theta}{\lambda^S + 2\mu^S} \end{cases} \tag{19}$$

Formally, the behaviour at infinity can be written

$$\widehat{\widetilde{W}}^1(y_1, y_2) \sim D^0 \frac{1}{\rho} \underline{t}^{-1}(\theta) \tag{20}$$

where $\sim$ means "behaves like at infinity" and D^0 is the corresponding generalized stress intensity factor. The explanation for the index 0 will be given further. It must be pointed out that the computation of $\widehat{\widetilde{W}}^1(y_1, y_2)$ can be done once and for all by a FEA as well as the calculation of D^0, regardless of the loading and the geometry of the specimens.

5. The outer expansion

Applying once again matching rules, the behaviour at infinity of the inner terms defined by Eqs. (18) and (20) must match with the outer expansion. First, it imposes the second term of (2) to split into

$$\begin{cases} U_1^e(x_1, x_2) = U_1^0(x_1, x_2) + Te\left(\pm A/2 + F_1(x_1, x_2) + \widehat{U}_1^1(x_1, x_2)\right) + \dots \\ U_2^e(x_1, x_2) = U_2^0(x_1, x_2) + Te\left(F_2(x_1, x_2) + \widehat{U}_2^1(x_1, x_2)\right) + \dots \end{cases} \tag{21}$$

where $\underline{F}(x_1, x_2)$ is defined by (17) in which r replaces ρ. In (21)$_1$ the sign $+$ is used in the right part of Ω^0 (Fig. 2(b)), i.e. for $x_1 \geqslant 0$, and vice versa.

As a consequence, the first corrective term in (2) is solution to a problem with an opening jump through the middle line Γ. This is not surprising, in Ω^0 the area occupied by the solder is replaced by the substrate which is generally stiffer. The elongation associated with $\underline{U}^0$ is then locally lower than the actual one and the complementary term corrects this inaccuracy by a discontinuity, i.e. a jump in the horizontal displacement. Vice versa there is an overlapping if the interphase is stiffer than the substrate. The jump or the overlapping is not contradictory with a mechanical behaviour, the term $e\underline{U}^1$ is a small correction to $\underline{U}^0$ that has no special mechanical meaning.

In addition to this jump there is a point force contribution, it accounts for the incompatible necking effects between substrate and solder in the domain Ω^0 where the thin solder layer is neglected. Under tension, the solder shrinks more than the substrate and pull on it. Fig. 6 summarizes the behaviour of the two leading terms $\underline{U}^0$ and $\underline{U}^1$ of the outer expansion near the origin O.

Another term theoretically appears in the form $e \ln e$ but it is multiplied by an irrelevant constant. The displacement field $\widehat{\underline{U}}^1(x_1, x_2)$ is solution to a well-posed problem, it fulfils stress free boundary conditions on the lower face of the specimen and appropriate boundary conditions derived from the discontinuity constant A and the point force $\underline{F}(x_1, x_2)$ elsewhere (where the logarithmic term is not singular).

Going further in the matching procedure, matching rules provide the next term $\underline{U}^2$ of the outer expansion (2) and its splitting according to (20)

$$\underline{U}^e(x_1, x_2) = \underline{U}^0(x_1, x_2) + Te\underline{U}^1(x_1, x_2) + TD^0 e^2 \underline{U}^2(x_1, x_2) + \dots \tag{22}$$

with

$$\underline{U}^2(x_1, x_2) = \frac{1}{r} \underline{t}^{-1}(\theta) + \widehat{\underline{U}}^2(x_1, x_2)$$

The displacement field $\widehat{\underline{U}}^2(x_1, x_2)$ is also solution to a well-posed problem. It fulfils stress free boundary conditions on the lower face of the specimen and appropriate boundary conditions derived from $1/r \underline{t}^{-1}(\theta)$ elsewhere (where this term is not singular).

6. Nucleation of a crack at the interface

The end of the solder layer is a privileged site for crack nucleation. The existence of a singular point leads to a stress concentration at the intersection between the interface and the free edge. As observed in the experiments, the only plausible mechanism seems to be a crack starting from or close to the free edge and growing along the interface (Fig. 7). We assume that its length ℓ at initiation is of the same order or smaller than the layer thickness e. In the stretched domain the dimensionless crack length is $\xi = \ell/e$. Otherwise, if ℓ is by far much larger than e, the expansions should be carried out first with respect to ℓ (and then with respect to $1/\xi = e/\ell \ll 1$), in this case the solder layer would play a minor role in the fracture process due to its small thickness compared to the crack length and a model with a weak virtual interface Γ is enough.

The function $\widehat{\widetilde{W}}^1(y_1, y_2)$ in (8) must now fulfil additional stress free boundary conditions on the two faces of the nucleated crack, thus a new condition must be added to (16)

$$\hat{\sigma}_{12}(y_1, y_2) = 0; \hat{\sigma}_{11}(y_1, y_2) = -T \quad \text{for}$$
$$y_1 = -1/2 \pm \quad \text{and} \quad 0 \leqslant y_2 \leqslant \xi \tag{23}$$

where signs $+$ and $-$ denote respectively the right and left faces of the new crack. This condition do not introduce new difficulties, the resultant force remains the same (condition (23) do not introduce any resultant force or moment), thus the behaviour at infinity of this solution is still defined by (17) and (19), then

$$\widehat{\widetilde{W}}^1(y_1, y_2) \sim D^\xi \frac{1}{\rho} \underline{t}^{-1}(\theta) \tag{24}$$

In the equations, the main difference prior to crack nucleation and following this event lies in the generalized stress intensity factors D^0 and D^ξ. In the first case, FEA are carried

5
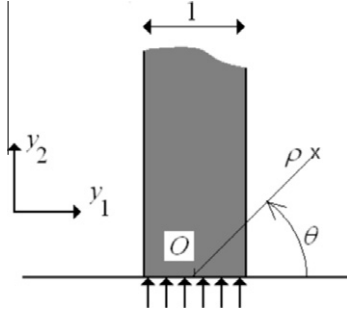
Fig. 5. The unbounded half space spanned by y_1 and $y_2 > 0$ and the special loading (16) for the function $\widehat{\underline{W}}^1(y_1, y_2)$.
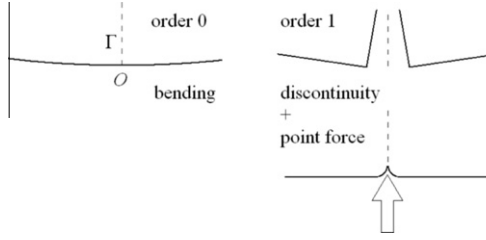
Fig. 6. Schematic view of the behaviour of the two leading terms of the outer expansion (21). (a) $\underline{U}^0$: pure bending, (b) $\underline{U}^1$: discontinuity plus point force.
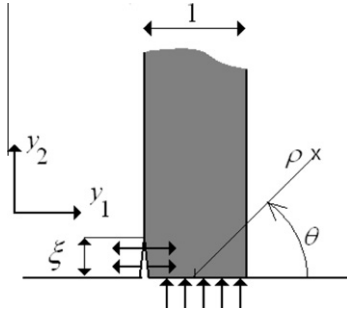
Fig. 7. Solder failure and the corresponding loading for the term $\widehat{\underline{W}}^1(y_1, y_2)$, the initial vertical loading (16) along the bottom face of the solder layer and the horizontal loading T on the two faces of the crack.

out on a crack free domain (Fig. 5) whereas its geometry embeds a crack in the latter one (Fig. 7). The outer expansion Eq. (22) has to be modified accordingly, simply replacing D^0 by D^ξ.

From this point of view (i.e. the function D^ξ), there is not much difference between a crack at the interface or inside the joint or even slightly outside in the substrate. The difference will come later when the properties at failure will be taken into account, they can differ dramatically depending on the location of the crack, in the SiC substrate, in the solder material or along the interface.

As mentioned above for D^0 the calculation of D^ξ can also be done once and for all, regardless of the loading and the geometry of the specimens.

7. The energy release rate for the interface crack

The change in potential energy δW^p between the two states (i.e. prior to and following the crack nucleation) can be written using a path independent integral (Leguillon, 1993; Labossiere and Dunn, 1999). To this aim, let us denote respectively $\underline{U}^{e0}(x_1, x_2)$ and $\underline{U}^{e\ell}(x_1, x_2)$ the solutions prior and following the crack nucleation, then

$$\delta W^p = \Psi(\underline{U}^{e\ell}, \underline{U}^{e0})$$
$$= \frac{b}{2} \int_\Phi [\sigma(\underline{U}^{e\ell})\underline{n}\underline{U}^{e0} - \sigma(\underline{U}^{e0})\underline{n}\underline{U}^{e\ell}]ds \tag{25}$$

where b is the specimen thickness (plane strain assumption) and where Φ is any contour encompassing the origin in the domain Ω^0 and starting and finishing at the bottom stress free edge of the specimen (Fig. 2), the vector $\underline{n}$ is its normal pointing toward the origin. The integral Ψ is path independent for any displacement fields fulfilling the balance equations. Substituting the outer expansions of the two terms in this integral gives

$$\delta W^p = e^2(D^\xi - D^0)T\Psi(\underline{U}^2, \underline{U}^0)b + \dots \tag{26}$$

and the incremental energy release rate derives immediately

$$G = -\frac{\delta W^p}{\ell b} = e\frac{D^\xi - D^0}{\xi}T\Psi(\underline{U}^0, \underline{U}^2) + \cdots \tag{27}$$

Here ℓb is the surface of the newly created crack. Using the expansion (3) for $\underline{U}^0(x_1, x_2)$, the splitting (22) for $\underline{U}^2(x_1, x_2)$ and some properties of the integral Ψ lead finally to (Leguillon and Sanchez-Palencia, 1987)

$$G = e\frac{D^\xi - D^0}{\xi}T^2\Psi(\underline{t}^1, \underline{t}^{-1}) + \cdots = e\,g(\xi)\,T^2 + \cdots \tag{28}$$

with

$$g(\xi) = \frac{D^\xi - D^0}{\xi}\Psi(\underline{t}^1, \underline{t}^{-1})$$

Here $\Psi(\underline{t}^1, \underline{t}^{-1})$ is a constant since the two functions $\underline{t}^1$ and $\underline{t}^{-1}$ are well known (see (4) and (19)). The function $g(\xi)$ (MPa^{-1}) depend on the geometry of the perturbation, i.e. the length of the crack (it should also weakly depend on the location of the crack but only one mechanism has been retained herein: the failure of the interface). Varying ξ, it is observed by a FEA that the function $g(\xi)$ is close to a linear one
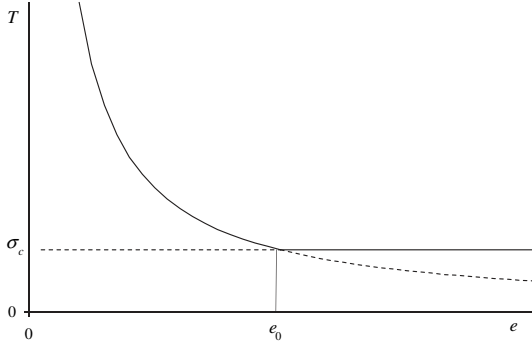
$$g(\xi) \approx 4.4\ 10^{-6} \times \xi \tag{29}$$

## 8. The interface fracture criterion

Respectively energy and stress based, two criteria are often invoked to predict failure either separately in general or in conjunction in some other cases (Leguillon, 2002). They write

$$-\delta W^P \geqslant G_c\ell b \quad \text{and} \quad T \geqslant \sigma_c \tag{30}$$

where G_c and σ_c denote the toughness and the tensile strength of the interface. The right hand side member $G_c\ell b$

6

Fig. 8. Transition between two regimes, the energy driven regime below the transition thickness e_0, the stress driven regime above (horizontal line).
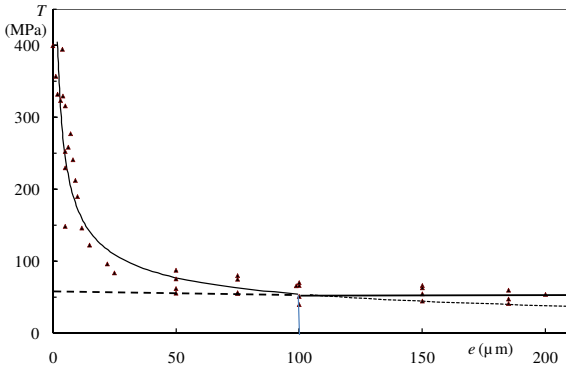
Fig. 9. Comparison between prediction (31) of the tensile stress at failure (solid line) and experiments conducted on specimens using CEA0 (triangles). Below the transition point it is energy driven and stress driven above.

is the energy consumed to create a crack with surface ℓb. Then, using (28), it comes from $(30)_1$

$$eg(\xi)T^2 \geqslant G_c \Rightarrow T \geqslant \sqrt{\frac{G_c}{e\,g(\xi)}} \tag{31}$$

At this stage, we make the strong but reasonable assumption that the crack length ℓ at initiation varies with the thickness e. For simplicity we suppose that it is proportional, then $g(\xi)$ and hence ξ are constant (note that the dimensionless crack length ξ is still unknown in (31)). The validity of such an assumption is corroborated by the forthcoming comparison with experimental results (Figs. 9 and 10). Other assumptions, especially ℓ independent of e, lead to conclusions which are not consistent with the experimental observations.

The present case seems very similar to that of the transverse cracking initiation in cross-ply laminates (Parvizi et al., 1978). The failure condition splits into two parts, the energy driven regime if e is small enough (Eq. (31)) and the stress driven regime $T = \sigma_c$ if e is large (Leguillon, 2002) (Fig. 8).

The transition point e_0 is obtained if the two conditions (30) are simultaneously fulfilled therefore
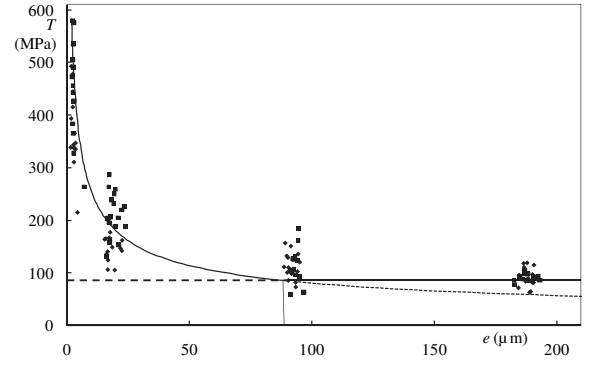
Fig. 10. Comparison between prediction (31) of the tensile stress at failure (solid line) and experiments on specimens using CEA1 (squares) and CEA2 (diamonds). Below the transition point it is energy driven and stress driven above.

$$e_0 = \frac{1}{g(\xi)}\frac{G_c}{\sigma_c^2} \tag{32}$$

Figs. 9 and 10 show the tensile stress at failure along the bottom face of the specimen derived from measurements of the failure remote load (see Eq. (1)) compared to the theoretical prediction (31). The experimental points come from 3 families of test conducted on the 2 grades of solder CEA1 and CEA2 to which were added items collected in databases (CEA0). They all correspond to a failure of the interface. We recall that a failure in the substrate was observed in some few cases corresponding to very thin layers of solder.

Values of T seem to tend toward an asymptotic limit around $\sigma_c \simeq 54$ MPa (the point at the far right of the graph, Fig. 8) for CEA0. The transition point can be estimated at $e_0 = 100$ μm. CEA1 and CEA2 give the asymptotic value $\sigma_c \simeq 84$ MPa, $e_0 = 92$ μm. This asymptotic value can be retained as the tensile strength of the interface defined in $(30)_2$.

The solder toughness K_{Ic} of CEA1 and CEA2 has been estimated to 1.5 MPa m$^{1/2}$ by nano indentation leading to $G_c = 0.12\ 10^{-4}$ MPa m (12 J m^{-2}), this value is chosen for the interface solder/substrate toughness. Indeed it cannot be larger than that of the weaker of the two adjacent materials; in any case this value is an upper bound of the actual interface toughness which is very difficult to estimate. As a consequence, for CEA1 and CEA2, the unknown parameter in (32) can be estimated: $\xi = \ell/e \approx 4$. It must be pointed out that this length does not have much physical meaning. It is simply a length below which no energy balance holds true (see (30)) and then no crack arrest can be observed.

For e below the transition point e_0 the tensile stress at failure depends on the layer thickness as $1/\sqrt{e}$. The Log–Log diagram of T vs. e fits with a linear function of the form

$$\ln(T) = -\frac{1}{2}\ln(e) + z \tag{33}$$

where z is the only degree of freedom determined by a least square method leading finally to the approximations exhibited on Figs. 9 and 10. Of course these curves are bounded from above by the tensile strength of the SiC substrate as $e \to 0$.

9. Conclusion

The representation of the behaviour of a structure embedding a thin joint under the form of asymptotic expansions is well known for a long time as long as interior points are concerned. Literature becomes sparser when the boundary conditions and the disturbances present in the area where the bonding layer meets the free edge must be taken into account. We showed here that the outer expansion has a classical form to which is added a logarithmic term representing a point force which intensity depends strongly on the contrast between the materials forming the substrate and the solder and in particular on the necking properties of the two materials.

However, this term plays no role in the failure criterion which takes a particularly simple form. It has two branches, one is governed by an energy condition, depending on $1/\sqrt{e}$ for small thicknesses and the other governed by a stress condition, independent of e for larger thicknesses of the solder layer. The identification made on a large number of measurements is mainly there to show the correctness of formula (31). Indeed, there is a very good agreement between the experiments and the theoretical curve.

Nevertheless, to be predictive, the constant z in (33) must be identified without going through the least square procedure (i.e. through a large number of tests). It can be done as follows: the tensile stress at failure T_m is measured from a test carried out for a given joint thickness e_m, then according to Eq. (33), z and finally T at failure noted T_f for any bonding layer thickness are determined by

$$z = \ln(T_m\sqrt{e_m}) \Rightarrow T_f = T_m\sqrt{\frac{e_m}{e}} \tag{34}$$

provided points are located in the energy driven branch (i.e. for $e_m \leqslant e_0$ and $e \leqslant e_0$). While it is difficult to determine the transition point, we see in Figs. 9 and 10 that considering this energy condition everywhere does not lead to large inaccuracies within the thicknesses range analyzed here. Moreover, a measured value of T_m not too far from the tensile strength of SiC means that e_m is small and below e_0, then this approach provides a conservative calculation that underestimates the strength of the structure in the stress governed branch.

Thermal residual stresses due to the process for making the joint have not been explicitly considered in this study. Tests conducted at high and low temperatures failed to clearly demonstrate this role, as several authors have found, even if the thermal expansion coefficients are significantly different. However, in the present case, it is likely that their effects whatever they are would simply shift the curves 9 and 10 without changing their shape. Thus, it is transparent to the above reasoning which remains valid since it is based on the identification of e_m and T_m at an experimental point of the curve.

Acknowledgments

References

ASTM C1211-02, 2008. Standard Test Method for Flexural Strength of Advanced Ceramics at Elevated Temperatures.

Bath, D.A., Spain, D., Ness, E., Williams, S., Bougoin, M., 2005. Evaluation of segmented and brazed mirror assemblies. SPIE Proceedings Series, Optical Materials and Structures Technologies 5868, 805.1–805.8.

Cockeram, B.V., 2005. Flexural strength and shear strength of silicon carbide to silicon carbide joints fabricated by a Molybdeum diffusion Bonding Technique. J. Am. Ceram. Soc 88 (7), 1892–1899.

Gasse, A., 2003. Method for assembling parts made of materials based on SiC by non-reactive refractory brazing, brazing composition, and joint and assembly obtained by said method, US2003/0038166-A1 patent.

Gasse, A., Coing-Boyat, G., Bourgeois, G., 2003. Method using a thick joint for joining part in SiC-based materials by refractory brazing and refractory thick joint thus obtained, US.6221.499-B1 patent.

Haboussi, M., Dumontet, H., Billoët, J.L., 2001. On the modelling of interfacial transition behaviour in composite materials. Comput. Mater. Sci. 20, 251–266.

Katoh, Y., Kotani, M., Kohyama, A., Montorsi, M., Salvo, M., Ferraris, M., 2000. Microstructure and mechanical properties of low-activation glass-ceramic joining and coating for SiC/SiC composites. J. Nucl. Mater., 283–287, 1262–1266.

Labossiere, P.E.W., Dunn, M.L., 1999. Stress intensities at interface corners in anisotropic bimaterials. Eng. Fract. Mech. 62, 555–575.

Leguillon, D., 1993. Asymptotic and numerical analysis of a crack branching in non-isotropic materials. Eur. J. Mech. A/Solids 12 (1), 33–51.

Leguillon, D., 1995. Concentration de contraintes et rupture dans les joints adhésifs. Actes du Deuxième Colloque National en Calcul des Structures. Hermès.

Leguillon, D., 2002. Strength or toughness? A criterion for crack onset at a notch. Eur. J. Mech. – A/Solids 21, 61–72.

Leguillon, D., Abdelmoula, R., 2000. Mode III near and far fields for a crack lying in or along a joint. Int. J. Solids Struct. 37 (19), 2651–2672.

Leguillon, D., Sanchez-Palencia, E., 1987. Computation of Singular Solutions in Elliptic Problems and Elasticity. John Wiley & Son, New York, and Masson, Paris.

Leguillon, D., Sanchez-Palencia, E., 1990. Approximation of a two dimensional problem of junctions. Comput. Mech. 6, 435–455.

Lewinsohn, C.A., Singh, M., Shibayama, T., Hinoki, T., Ando, M., Katoh, Y., Kohyama, A., 2000. Joining of silicon carbide composites for fusion energy applications. J. Nucl. Mater., 1258–1261.

NF EN 843-1, 2007. Propriétés mécaniques des céramiques monolithiques à température ambiante. – Partie 1: détermination de la résistance à la flexion. French standard.

Nguetseng, N., Sanchez-Palencia, E., 1985. Stress concentration for defects distributed near a surface. In: Ladeveze, P. (Ed.), Local Effects in the Analysis of Structures. Elsevier, Amsterdam, pp. 55–74.

Nguyen, L.M., 2011. Comportement mécanique d'une jonction brasée SiC/BraSiC/SiC – critère de dimensionnement, PhD thesis, University Pierre et Marie Curie, Paris, France.

Parvizi, A., Garrett, K.W., Bailey, J.E., 1978. Constrained cracking in glass fibre-reinforced epoxy cross-ply laminates. J. Mater. Sci. 13, 195–201.

Riccardi, B., Nannetti, C.A., Woltersorf, J., Pippel, E., Petrisor, T., 2002a. Brazing of SiC and SiCf–SiC composites performed with 84Si–16Ti eutectic alloy: microstructure and strength. J. Mater. Sci. 37, 5029–5039.

Riccardi, B., Nannetti, C.A., Woltersdorf, J., Pippel, E., Petrisor, T., 2002b. High temperature brazing for SiC and SiC–SiC ceramic matrix composites. Ceram. Trans. 144, 311–332.

Rodriguez, G., Robin, J.C., Cachon, L., Tochon, P., Bucci, P. Chaumat, V., Gillia, O., Terlain, A., 2007. Preliminary design and development of a key component of the Iodine Sulfur thermochemical cycle: the SO3 decomposer, Société Française d'Energie Nucléaire – International Congress on Advances in Nuclea Power Plants – ICAPP 2007, in The Nuclear Renaissance at Work, 4, pp. 2580–2586.

Singh, M., 1997. A reaction forming method for joining of silicon carbide based ceramics. Scr. Mater. 37 (8), 1151–1154.

Timoshenko, S., Goodier, J.N., 1951. Theory of Elasticity, second ed. Mc Graw Hill Co., New York.